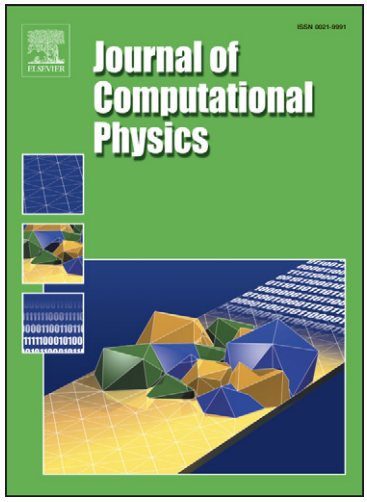

A semi-intrusive deterministic approach to uncertainty quantification in non-linear fluid flow problems

R. Abgrall, P.M. Congedo

PII: S0021-9991(12)00426-3
DOI: http://dx.doi.org/10.1016/j.jcp.2012.07.041
Reference: YJCPH 4146

To appear in: *Journal of Computational Physics*

Received Date: 16 October 2011
Revised Date: 21 June 2012
Accepted Date: 26 July 2012

Please cite this article as: R. Abgrall, P.M. Congedo, A semi-intrusive deterministic approach to uncertainty quantification in non-linear fluid flow problems, *Journal of Computational Physics* (2012), doi: http://dx.doi.org/10.1016/j.jcp.2012.07.041

A semi-intrusive deterministic approach to uncertainty quantification in non-linear fluid flow problems

R. Abgrall[1] and P. M. Congedo

Bacchus Team Project
Domaine de Voluceau Rocquencourt - B.P. 105 78153 Le Chesnay, France
and
Institut de Mathématiques de Bordeaux, Université de Bordeaux
351 Cours de la Libération, 33400 Talence, France

Abstract

This paper deals with the formulation of a semi-intrusive (SI) method allowing the computation of statistics of linear and non linear PDEs solutions. This method shows to be very efficient to deal with probability density function of whatsoever form, long-term integration and discontinuities in stochastic space.

Given a stochastic PDE where randomness is defined on Ω, starting from (i) a description of the solution in term of a space variables, (ii) a numerical scheme defined for any event $\omega \in \Omega$ and (iii) a (family) of random variables that may be correlated, the solution is numerically described by its conditional expectancies of point values or cell averages and its evaluation constructed from the deterministic scheme. One of the tools is a tessellation of the random space as in finite volume methods for the space variables. Then, using these conditional expectancies and the geometrical description of the tessellation, a piecewise polynomial approximation in the random variables is computed using a reconstruction method that is standard for high order finite volume space, except that the measure is no longer the standard Lebesgue measure but the probability measure. This reconstruction is then used to formulate a scheme on the numerical approximation of the solution from the deterministic scheme. This new approach is said semi-intrusive because it requires only a limited amount of modification in a deterministic solver to quantify uncertainty on the state when the solver includes uncertain variables.

The effectiveness of this method is illustrated for a modified version of Kraichnan-Orszag three-mode problem where a discontinuous pdf is associated to the stochastic variable, and for a nozzle flow with shocks. The results have been analyzed in terms of accuracy and probability measure flexibility. Finally, the importance of the probabilistic reconstruction in the stochastic space is shown up on an example where the exact solution is computable, the viscous Burgers equation.

Keywords: Uncertainty quantification, continuous and discontinuous pdf, finite volume method, long time integration, nozzle flow, shocked flows.

1. Introduction

There are many situations where one wants to estimate some statistics on the solution of a PDE. Consider the flow around an aircraft for example. The boundary conditions (inflow Mach number, Reynolds number, some geometrical parameters) may only be known approximately either in a nozzle flow or a true flight. In hypersonic, the equation of state or the viscous model play an important role and they are sometimes known very approximately. The same is true for multiphase flows. One may also wish to "extrapolate" experimental results which are partially known to flow conditions that are not contained in the experimental data base: what is the confidence one may have ? The question is not only to know the sensitivity of the solution, but

[1]Corresponding author

also to to understand the importance (i.e. the weight) of these variations. In other terms, assuming the likely-hood of relative variations, how can we weight their influence on the solution ?

Several stochastic methods have been proposed in literature. The Monte Carlo method (MCM) and its variants [16] are the most popular approach to model uncertainty because of its versatility, but it is too expensive in order to be used in CFD stochastic computations: each sample corresponds to a full CFD run ! It becomes competitive with respect to other methods only if high dimensional probability space is considered since the order of convergence is independent of the number of independent random parameters. Several stochastic methods are based on dividing probability space into multiple sub-domains and by using a polynomial approximation of the response surface [24, 33]. Other approaches are the intrusive [15, 34, 7, 10] and non-intrusive [22, 23, 27] formulations relying on Polynomial Chaos expansion of the random variables. Polynomial Chaos methods, first introduced by Ghanem and Spanos [15] appear to be a good alternative to statistical methods for uncertainty quantification. In 2002, Xiu and Karniadakis [34] introduced Generalized Polynomial Chaos. It was demonstrated that in order to achieve optimal convergence, the type of orthogonal polynomials in the chaos expansion should correspond to the properties of the stochastic process based on the association between probability density functions (pdf) and weighting functions. In [30], Wan and Karniadakis have developed a multi-element polynomial chaos method. The main idea is to adaptively decompose the space of random inputs into multiple elements and employ polynomial chaos expansion at element level.

For long integration problems, non-intrusive methods shows very good results [11]. Intrusive formulations, like Polynomial Chaos, can suffer of loss of accuracy for longer time [24, 18, 31]. A possible cure has been proposed by Gerristma *et al.* in [13], where adaptation of the set of orthogonal polynomials with respect to the changing pdf removes the error with respect to long time integration.

Another important point in UQ community is the possibility to have a numerical method allowing to treat any form of the pdf, aiming at using experimental pdf taken directly from the experience. In the case of non-intrusive methods, the idea is to sample the input random space by very specific random events that are associated to the Gaussian points of the integration formulation that corresponds to the expectancy. This indicates that one can consider *a priori* any type of pdf and the only thing to do is to evaluate these quadrature points. In practice this means that one has to compute an orthogonal (with respect to the pdf) polynomial basis, and to evaluate the zeros of the highest degree polynomial. Unfortunately, this can be a very tricky and difficult task in many circumstances: if it is known that the zeros of these polynomials are distinct, it is not at all easy to accurately compute the roots of a polynomial in general, and here accuracy is a must. Moreover, this strategy assumes that the input random variables are independent.

For shock-dominated flows, oscillations due to Gibbs phenomenon can appear close to the discontinuities. Several formulations have been introduced to solve this problem, see for example [26] for a detailed review, where a new method has been proposed by using the entropy variables which is developed on the polynomial basis by performing a Galerkin projection.

In this paper, we present a new approach, particularly suited for flow problems, proposing possible cures for several important aspects in uncertainty quantification, as long-time integration problems, flexibility with respect to the form of the pdf, the independence of the random variables and stochastic shock discontinuity.

The outline of this paper is as follows. In section 2, the basic idea of semi-intrusive method is explained. Moreover, error analysis is shown up and implementation details are given. In section 3, the SI method is applied to Kraichnan-Orszag problem, to a nozzle flow with discontinuity and to the viscous Burgers equation. Finally, in section 4, conclusions are drawn.

2. Principles of the method

2.1. General formulation of the method

Let us start from some model represented by a PDE, say

$$\mathcal{L}(u) = 0, \tag{1}$$

defined in a domain K of $\mathbb{R}^d$ subjected to boundary conditions, and if needed initial conditions. Since the discussion of this section is formal, we put the different initial and boundary conditions of the problem in the symbol $\mathcal{L}$. The operator $\mathcal{L}$ depends in some way on parameters[2], that in many cases are not well known. Hence we assume they are random variables defined on some universe Ω equipped with a family $\mathcal{B}$ of measurable sets and a measure $d\mu$. We assume that these random variables are measurable with respect to the measure $d\mu$. Hence our problem can formally be seen as a "stochastic" PDE of the type

$$\mathcal{L}(u, X) = 0, \tag{2}$$

defined in a domain K of $\mathbb{R}^d$, subjected to initial and boundary conditions, and where X is a random variable defined on Ω. By abuse of language, we use the same notation $\mathcal{L}$ for the problem. The operator $\mathcal{L}$ depends on $u := u(x, t, X)$ or $u := u(x, X)$, depending whether the problem is time dependent or not, and $X := X(\omega)$. Here, $x \in \mathbb{R}^d$ for $s \in \{1, 2, 3\}$, $t \in \mathbb{R}^+$ are the usual space and time parameters, and the event ω belongs to Ω. The random variable may also depend on space and time, as well as the measure $d\mu$. The technique we develop in this paper could in principle be extended to this case but the discussion is beyond the scope of this paper, for simplicity of exposure.

We identify Ω to some subset of $\mathbb{R}^s$, s being the number of random parameter to define X. Hence, for any measurable real valued function,

$$E(f(X)) = \int_{\mathbb{R}^s} f(x_1, \ldots, x_s) d\mu(x_1, \ldots, x_s)$$

or more simply

$$E(f(X)) = \int_{\mathbb{R}^s} f(x_1, \ldots, x_s) d\mu.$$

This does not mean that the measure $d\mu$ is obtained by tensorisation, the components x_j can be correlated. Thus we can also see (2) as a problem defined on a subset K' of $\mathbb{R}^d \times \mathbb{R}^s$.

For any realization of Ω, we assume to be able to solve the following approached deterministic form of (2) in space and time, by some numerical method:

$$\mathcal{L}_h(u_h, X(\omega)) = 0. \tag{3}$$

Our approach to approximating the solution of (2) starts with discretizing the probability space Ω. We construct a partition of Ω, i.e. a set of Ω_j, $j = 1, \ldots, N$ that are mutually independent

$$\mu(\Omega_i \cap \Omega_j) = 0 \text{ for any } i \neq j \tag{4}$$

and that cover Ω

$$\Omega = \cup_{i=1}^{N} \Omega_i. \tag{5}$$

We assume $\mu(\Omega_i) = \int_{\Omega_j} d\mu > 0$ for any i. We wish to approximate the solution of (2) by the average conditional expectancies $E(u_h|\Omega_j)$

$$E(u_h \mid \Omega_j) = \frac{\int_{\Omega_j} u_h d\mu}{\int_{\Omega_j} d\mu} \tag{6}$$

from the knowledge of the operator $\mathcal{L}_h$.

Let us illustrate how this idea can be made effective. If an iterative technique is used to solve (3), as it is often the case, a deterministic solution can be written as

$$u_h^{n+1} = \Im(u_h^n) \tag{7}$$

[2]for example the equation of state, or the parameters of a turbulent model, to give examples in fluids

where the operator $\Im$ is a succession of additions, multiplications and function evaluations. In (7), the index n can be the index of the iteration *stricto sensu*, or the index of the time step in the case of an explicit method for a time dependent problem, etc. This leads to

$$E\left(u_h^{n+1} \mid \Omega_j\right) = E\left(\Im\left(u_h^n\right) \mid \Omega_j\right). \tag{8}$$

This scheme is fully defined if $E\left(\Im\left(u_h^n\right) \mid \Omega_j\right)$ can be evaluated. We show how to do that in sections 2.2 and 2.3. Thus we are able to construct a sequence $\left(E\left(u_h^{n+1} \mid \Omega_j\right)\right)_{n\geq 0}$. If the problem is steady and *if this sequence converges in some sense*, the limit is the sought solution. In the case of time dependent problems, (8) represents an approximation of the conditional expectancy at time t_{n+1}. In the case of explicit/implicit methods, as for dual time stepping, the interpretation of (8) can easily be done in the relevant context.

Once, conditional expectancy is computed, it is possible to compute mean and variance by means of the following definitions :

$$\text{Mean} = \sum_{\Omega_j} u_h^n, \qquad \text{Variance} = \sum_{\Omega_j} \int_{\Omega_j} (\text{Mean} - u_h^n)^2 d\mu$$

and even an approximation of the pdf of u_h^n.

2.2. Consistency of the method

Given the conditional expectancies $E\left(X \mid \Omega_j\right)$, can we estimate for a given f, $E(f(X))$?

The idea is the following: For each Ω_j, we first define a stencil, i.e. a set $\mathcal{S}_i = \{\Omega_j\}_{j\in I_i}$ with $\Omega_i \in \mathcal{S}_i$ and we wish to evaluate a polynomial $P_i \in \mathbb{R}\left[x_1, \cdots, x_n\right]$ of degree p such that

$$E\left(X \mid \Omega_j\right) = \frac{\int_{\mathbb{R}^n} 1_{\Omega_j}\left(x_1, \cdots, x_n\right) P\left(x_1, \cdots, x_n\right) d\mu}{\mu\left(\Omega_i\right)} \qquad \text{for } j \in \mathcal{S}_i. \tag{9}$$

This problem is reminiscent of what is done in finite volume schemes to compute a polynomial reconstruction in order to increase the accuracy of the flux evaluation thanks the MUSCL reconstruction. Among the many references that have dealt with this problem, with the Lebesgue measure $dx_1 \dots dx_n$, one may quote [17] and for general meshes [8, 2]. A systematic method for computing the solution of problem (9) is given in [5].

We can easily derive a technical condition that guaranties that the problem (9) has a unique solution. We can index the set of multi-indices $\{\alpha = (\alpha_1, \cdots, \alpha_n)\}_{|\alpha|\leq p}$ with $|\alpha| := \sum_{i=1}^n \alpha_i$ as $\alpha_1, \dots, \alpha_{N_p}$. Then we can define, for $x = (x_1, \dots, x_n)$, the monomial $x^\alpha := x_1^{\alpha_1} \dots x_n^{\alpha_n}$. The technical condition that ensure a unique solution to problem (9) is that the Vandermonde–like determinant

$$\Delta = \det\left(E(x^{\alpha_i}|\Omega_j)\right)_{0\leq i\leq N_p, j\in\mathcal{S}_i}. \tag{10}$$

is non zero. A necessary condition, in 1D, is that $\#\mathcal{S}_i \geq \frac{p(p+1)}{2}$. Similar, but more complex expressions of this type exist for multivariate polynomials.

Once the solution of (9) is known, we can estimate

$$E\left(f(X)\right) \approx \sum_{j=1}^{N} \int_{\Omega_j} f\left(P\left(x_1, \cdots, x_n\right)\right) d\mu \tag{11a}$$

by using a relevant quadrature formula in each Ω_j. For example, if $d\mu$ has a density in Ω_i, we can do

$$\int_{\Omega_j} f\big(P(x)\big) d\mu \approx \sum_{k=1}^{m_i} w_k^i f\big(P(x_k^i)\big) \tag{11b}$$

where the weights are the w_k^i and the quadrature points are the x_k^i. If $d\mu$ has no density, some the formula, depending on the structure of $d\mu$, must be used, but the principle stays the same.

We have the following approximation results : if $f \in C^1(\mathbb{R}^n) \cap L^1(\Omega, \mu)$ and X of classC^r, $r \geq p+1$ then

$$\left| E\left(f(X)\right) - \sum_{j=1}^{N} \int_{\mathbb{R}^n} 1_{\Omega_j}\left(x_1, \cdots, x_n\right) f\left(P\left(x_1, \cdots, x_n\right)\right) d\tilde{\mu} \right| \leq \max ||D^{p+1}X||_\infty \max_{\Omega_i} \min_{\omega_i \in \Omega_i} E(||(\omega - \omega_i)^{p+1}||\,|\Omega_i).$$

for a set of regular stencils. The proof of this results is given in the appendix Appendix A.

Remark 2.1. *We notice that we never need to make any additional assumption on the structure of X to evaluate P in* (9)*. In particular, its components can be correlated.*

2.3. Polynomial reconstruction

In this section, we provide explicit examples and applications of the reconstruction technique that we have abstractly sketched in the previous paragraph. Let us subdivide the space Ω into non overlapping measurable subsets. For the simplicity of exposure we will consider one source of uncertainty, thus the subsets can be identified to N intervals of $\mathbb{R}$ which are denoted by $\Omega_j = [\omega_{j-1/2}, \omega_{j+1/2}]$. The case of multiple sources can be considered in a similar way, for example as what is done for the ENO or WENO reconstruction methods. Examples of such methods are given in [2, 12, 19], among other references. Note that the subsets Ω_j, seen as subsets of $\mathbb{R}^n$ may well be unbounded, the only relevant information is that their *measure* $\mu(\Omega_j)$ is bounded. This is obviously the case because μ is a probability measure.

Let us describe in details what is done for one source of uncertainties. In the cell Ω_i, the polynomial $P_i \in \mathbb{P}^p(\mathbb{R})$ of degree p is fully described by a stencil $\mathcal{S}_i = \{\Omega_i, \Omega_{i_1}, \ldots, \Omega_{i_p}\}$ where the indices $i_1, \ldots i_p$ are all different and different of i. We have, by definition,

$$E(P_i|[\omega_{j-1/2}, \omega_{j+1/2}]) = E(u|[\omega_{j-1/2}, \omega_{j+1/2}]), \text{ for any } j \in \{i, i_1, \ldots, i_p\}.. \tag{12}$$

It is easy to see that there is a unique solution to that problem provided that the cells of $\mathcal{S}_i$ do not overlap, which is the case here.In the numerical examples, we consider three reconstruction mechanisms :

- a first order reconstruction: we simply take $\mathcal{S}_i = \{\Omega_i\}$ and the reconstruction is piecewise constant,
- An ENO reconstruction: The construction is done in two steps. We first evaluate two linear polynomials, and take the least oscillatory one. We introduce the average mid-points

$$\omega_l = E(\xi|\Omega_l).$$

1. For the cell Ω_i, we first evaluate two polynomials of degree 1. The first one, p_i^-, is constructed using the cells $\{\Omega_{i-1}, \Omega_i]\}$ and the second one, p_i^+, on $\{\Omega_i, \Omega_{i+1}\}$. The polynomial of degree 1 p_i^+ can be written as

$$p_i^+(\xi) = a_i^+\big(\frac{\xi - \omega_i}{\omega_{i+1} - \omega_i}\big) + b_i^+.$$

It has to satisfy the relations

$$E(p_i^+|\Omega_i) = E(u|\Omega_i) \text{ and } E(p_i^-|\Omega_{i-1}) = E(u|\Omega_{i-1}).$$

This leads to a 2×2 system that can be solved. Thanks to the definition of ω_i, we have $E(x - \omega_i|\Omega_i) = 0$ and thus it has a very simple structure:

$$\begin{pmatrix} 1 & 0 \\ 1 & 1 \end{pmatrix} \begin{pmatrix} b_i^+ \\ a_i^+ \end{pmatrix} = \begin{pmatrix} E(u|\Omega_i) \\ E(u|\Omega_{i+1}) \end{pmatrix} \tag{13}$$

that can be solved immediately. Similarly, the polynomial $p_i^-(\xi) = a_i^-\big(\frac{\xi - \omega_i}{\omega_{i+1} - \omega_i}\big) + b_i^-$ can be evaluated by solving (13) where the indices have been shifted of -1.

2. We choose the least oscillatory one, i.e. the one which realizes the oscillation $\min(|a_i^+|, |a_i^-|)$.

- a centered reconstruction: the stencil is $\mathcal{S}_{i+1/2} = \{\Omega_{i-1}, \Omega_i, \Omega_{i+1})$ and the reconstruction is piecewise quadratic. At the boundary of Ω, we reduce to degree one: we use the reduced stencils $\mathcal{S}_{1/2} = \{\Omega_{1/2}, \Omega_{3/2}\}$ for the first cell Ω_0 and $\mathcal{S}_{N-1/2} = \{\Omega_{N-1/2}, \Omega_{N-3/2}\}$ for the last cell Ω_{N-1}.

  For the internal cells, let us describe the computational algorithm. We chose to write the polynomials with the expansion

$$p(\xi) = a + b\frac{\xi - \omega_i}{\omega_{i+1} - \Omega_i} + c\left(\frac{\xi - \omega_i}{\omega_{i+1} - \Omega_i}\right)^2.$$

  We first compute the polynomial of degree 1 that matches $E(u|\Omega_i)$ and $E(u|\Omega_{i+1})$ in average, i.e we solve the system (13). Let us denote by p_i^+ this polynomial. Then, instead of evaluating p directly, we evaluate

$$q = p - p_i^+ = a' + b'\frac{\xi - \omega_i}{\omega_{i+1} - \Omega_i} + c'\left(\frac{\xi - \omega_i}{\omega_{i+1} - \Omega_i}\right)^2.$$

  The linear system has a nice structure

$$\begin{pmatrix} 1 & 0 & E\left(\left(\frac{\xi - \omega_i}{\omega_{i+1} - \Omega_i}\right)^2 |\Omega_i\right) \\ 1 & 1 & E\left(\left(\frac{\xi - \omega_i}{\omega_{i+1} - \Omega_i}\right)^2 |\Omega_{i+1}\right) \\ 1 & E\left(\frac{\xi - \omega_i}{\omega_{i+1} - \Omega_i}|\Omega_{i-1}\right) & E\left(\left(\frac{\xi - \omega_i}{\omega_{i+1} - \Omega_i}\right)^2 |\Omega_{i-1}\right) \end{pmatrix} \begin{pmatrix} a' \\ b' \\ c' \end{pmatrix} = \begin{pmatrix} 0 \\ 0 \\ E(u|\Omega_{i-1}) - E(p_i^+|\Omega_{i-1}) \end{pmatrix}$$

  which can easily be solved using the block structure, see [5]. This method is reminiscent of the Newton algorithm for lagrange interpolation.

Other choices are possible such as WENO-like interpolants. Again, these algorithms can be extended to several stochastic dimensions, the main step is to define a family of stencils. This can be carried out by defining a tessellation of cells as this has been done for ENO methods on unstructured meshes, see [2, 1] for example.

2.3.1. Numerical integration

Once the polynomial is reconstructed, we need to evaluate conditional expectancies. This amounts to perform numerical integrations over Ω_j. If $d\mu = \mu(\omega)d\omega$, this can be done thanks to a classical quadrature method, as the following third order Gaussian quadrature:

$$\int_a^b h(\omega)d\omega \approx \frac{b-a}{2}(h(\xi_1) + h(\xi_2)), \tag{14}$$

where $\xi_1 = \frac{a+b}{2} - \frac{b-a}{2}\frac{\sqrt{3}}{3}$ and $\xi_2 = \frac{a+b}{2} + \frac{b-a}{2}\frac{\sqrt{3}}{3}$.

In all the practical illustrations, we will use only one or two sources of uncertainty even though the method can be used for any number of uncertain parameters, this leading to other known problems such that the curse of dimensionality. Using classical quadrature formulas in multi-dimensional stochastic problem, the computational cost can increase exponentially [29], and others methods, as the sparse grid methods must be used [14, 21]. These methods are based on a linear combination of tensor product of one dimensional quadrature formulas.

Remark 2.2. *Of course, the structure of the quadrature formula depends on the measure $d\mu$ and the structure of the cells Ω_i. In all our computations, we are using cells that either intervals, quadrangles, or tensor products of interval more generally speaking. This does not mean that the measure needs a product of 1D measures. However, if the measure has a density, the most straightforward quadrature formula are those obtained by tensorisation of 1D formulas.*

2.4. 1D-1D Discretization

Fundamental concepts have been introduced in the previous sections, and we will now focus on a detailed discretization of an 1D-1D PDE. By "1D-1D", we mean one dimension in the geometric space and one dimension in probabilistic space. Let us consider the following equation

$$\begin{gathered}\frac{\partial u}{\partial t}+\frac{\partial f(u)}{\partial x}=S,\\ \text{Initial and/or boundary conditions,}\end{gathered} \tag{15}$$

defined in a domain $K = D \times \Omega \subset \mathbb{R}^2$, where $u := u(x, t, X(\omega))$, $S := S(x, t, X(\omega))$ is a source term and $t > 0$. The space parameter x is defined on $D \subset \mathbb{R}$, ω and X are respectively a random parameter and a random variable, defined on the probability space $(\Omega, d\mu)$ where $d\mu$ is the probability measure and $\Omega \subset \mathbb{R}$. The initial conditions, boundary conditions and the domain D may be random.

As explained previously in section 2.1, the discretization of (15) is based on two steps, the integration of the deterministic part of the system and the integration of the probabilistic part.

2.4.1. Deterministic formulation

We consider a spatial discretization for (15) with nodes points $x_i = i\Delta x$ where i belongs to some subset of $\mathbb{Z}$, a time step $\Delta t > 0$ and a set $t_n = n\Delta t$, $n \in \mathbb{N}$. The control volume is as usual the intervals $C_i = [x_{i-1/2}, x_{i+1/2}]$ with $x_{i+1/2} = (x_i + x_{i+1})/2$. We start from a finite volume scheme, and for the simplicity of exposure, we only consider a first order in time.

Thus we define the *deterministic scheme* (i.e. for any fixed ω) as

$$\begin{aligned}u_i^{n+1}(X(\omega)) = u_i^n(X(\omega))&\\ -\frac{\Delta t}{|C_i|}&\Big(F(u_{i+1}^n(X(\omega)), u_i^n(X(\omega))) - F(u_i^n(X(\omega)), u_{i-1}^n(X(\omega)))\Big)\\ &+\int_{C_i} S(x, t^n, X(\omega))\, dx,\end{aligned} \tag{16}$$

where F is a consistent approximation of the continuous flux f. The cell-averaged quantity is defined as

$$u_i^n(X(\omega)) = \frac{1}{|C_i|}\int_{C_i} u(x, t^n, X(\omega))dx. \tag{17}$$

2.4.2. Probabilistic formulation

The next step is the discretization of the probabilistic part of the equation, where the variables must be represented by their conditional expectancies. We consider a probabilistic discretization for (16) with nodes points $\omega_{j+1/2} = (j + 1/2)\Delta\omega$ where j belongs to some subset of $\mathbb{Z}$. The control volume is the intervals $\Omega_j = [\omega_{j-1/2}, \omega_{j+1/2}]$.

Thus we define the *probabilistic scheme* as

$$\begin{aligned}u_{i,j}^{n+1} = u_{i,j}^n - \frac{\Delta t}{|C_i|}&\Big(E(F(u_{i+1}^n, u_i^n)|\Omega_j) - E(F(u_i^n, u_{i-1}^n)|\Omega_j)\Big)\\ &+\frac{\Delta t}{|C_i|}E\Big(\int_{C_i} S(x, t^n, X(\omega))dx\Big|\Omega_j\Big)\end{aligned} \tag{18}$$

where the cell-averaged conditional expectancy is defined as

$$u_{i,j}^n = E(u_i^n(X)|\Omega_j) = \frac{1}{\mu(\Omega_j)}\int_{\Omega_j} u_i^n(X(\omega))d\mu(\omega). \tag{19}$$

2.4.3. Numerical flux evaluation

The expectancy of the numerical flux can be approximated as it is shown in section 2.2 by

$$E(F(u^n_{i+1}, u^n_i)|\Omega_j) \approx \frac{1}{\mu(\Omega_j)} \int_{\Omega_j} F(P^n_{i+1,j}, P^n_{i,j})\ d\mu, \tag{20}$$

where $P_{i,j}$ is a piecewise polynomial reconstruction of the probabilistic solution. Assuming that we require all polynomial reconstructions $P_{i,j}$ to have the correct cell average, we have

$$E(P_{i,j}|\Omega_j) = E(u_i|\Omega_j). \tag{21}$$

To achieve the second order accuracy, there are many reconstruction methods as it is shown in section 2.3.

Once reconstructed, the polynomial is injected in the numerical flux F. For the simplicity of the exposure let's formulate F thanks to the Roe's method:

$$F(P^n_{i+1,j}, P^n_{i,j}) = \frac{1}{2}\big(f(P^n_{i+1,j}) + f(P^n_{i,j}) - |A(P^n_{i+1,j}, P^n_{i,j})|(P^n_{i+1,j} - P^n_{i,j})\big) \tag{22}$$

where $|A(u^n_{i+1,j}, u^n_{i,j})|$ is the Jacobian matrix evaluated at the Roe's average, see [28] for details. Of course other methods are applicable.

2.4.4. Time stepping procedure

To finish with the discretization, the time step evolution is evaluated taking into account Δt_{Ω_j} for any realization Ω_j, which is obtained under classical CFL stability conditions. Thus the general time step is evaluated as

$$\Delta t = \min_{\Omega_j} \Delta t_{\Omega_j}. \tag{23}$$

2.4.5. Implementation issues

The deterministic scheme is sketched in algorithm 1 so that we can better see, by contrast, what are the modifications to introduced the semi-intrusive method sketched in algorithm 2. The algorithm 3 shows how to implement the stochastic resolution of the system (15).

As indicated, the modifications to the deterministic code are rather small. The first loop, on top of all the others, is a loop over the iterative parameter introduced in (8). It already exists in the deterministic method, see algorithm 1. The second loop, enclosed by the previous one, is a loop over the subsets Ω_j which also does not induce any modification of the code. In this loop, we first evaluate the reconstruction polynomials (in the stochastic direction), and for each quadrature points in (11), we evaluate the relevant data to be sent to the deterministic solver. Then we apply the deterministic solver $\Im$ on this datum. Once this loop is done, we evaluate U^{n+1} the vector made of $\{E(U^n|\Omega_j)\}_{\Omega_j}$ as in the quadrature formula (11). This method is further exemplified for (15) in algorithm 3.

2.5. Error analysis and estimated convergence

A discussion over the error analysis and the estimated convergence in reported in the appendix Appendix B. We consider two examples: the heat equation and the Burgers equations. The main lesson is that the error in evaluating $E(f(X))$ for smooth enough f and X is the sum of an error on the deterministic solver and an reconstruction error in the stochastic space,

$$\big|E(f(X)) - E(\tilde{f}(R))\big| \leq \text{approximation error on } \mathcal{L} + \text{ reconstruction error.} \tag{24}$$

where $E(\tilde{f}(R))$ represents the numerical approximation of $E(f(R))$ along the lines of (11).

3. Results

3.1. Kraichnan-Orszag problem

The Kraichnan Orszag (KO) three-modes problem has been introduced by Kraichnan [20] and Orszag [25]. It has been intensively studied to study the loss of accuracy of gPC expansion for problems involving long time integration. In [30], the exact solution is given, and different computations have been performed in [30, 32, 11, 13, 6, 21]. This problem is defined by the following system of nonlinear ordinary differential equations

$$\begin{aligned} \frac{\mathrm{d}y_1}{\mathrm{d}t} &= y_1 y_3, \\ \frac{\mathrm{d}y_2}{\mathrm{d}t} &= -y_2 y_3, \\ \frac{\mathrm{d}y_3}{\mathrm{d}t} &= -y_1^2 + y_2^2 \end{aligned} \tag{25a}$$

subject to stochastic initial conditions

$$y_1(0) = y_1(0;\omega), \qquad y_2(0) = y_2(0;\omega), \qquad y_3(0) = y_3(0;\omega). \tag{25b}$$

In general, uniform distributions are considered, except in [32] where beta and Gaussian distributions are also taken into account. The computational cost of SI method for the K-O problem is compared to that of other methods, namely a quasi-random Sobol (MC-SOBOL) sequence with 8 10^6 iterations, and a Polynomial Chaos Method (PC) with Clenshaw-Curtis sparse grid. The error in variance of y_1 is considered at a final time t_f of 50. We define the L^2 error between two numerically integrated functions $f_1(t_j)$ and $f_2(t_j)$, $j = 1, \cdots, n_t$, as:

$$\epsilon_{L^2} = \frac{\frac{1}{n_t}\sqrt{\sum_{j=1}^{n_t}\left(f_1(t_j) - f_2(t_j)\right)^2}}{\frac{1}{n_t}\sqrt{\sum_{j=1}^{n_t}\left(f_1(t_j)\right)^2}},$$

where f_1 is considered the Monte Carlo converged solution. Similarly, the L^∞ error is defined by

$$\epsilon_{L^\infty} = \frac{\max\limits_{j=1,\ldots,n_t} \left|f_1(t_j) - f_2(t_j)\right|}{\max\limits_{j=1,\ldots,n_t} \left|f_1(t_j)\right|}.$$

For different error levels, corresponding computational cost is given.

3.1.1. 1D KO problem

First, we study the 1D problem corresponding to initial conditions of the form

$$y_1(0) = 1.0, \qquad y_2(0) = 0.1\xi, \qquad y_3(0) = 0.0,$$

where ξ is a uniformly distributed random variable varying in $[-1, 1]$. We use SI, MC-SOBOL and PC method to compute the variance of y_1. In Table B.2, we show the results in terms of number of samples required to reach a prescribed error ϵ_{L^2}. The performance of the SI method are comparable and even better than PC method, at least on this problem.

Then, the same problem described previously has been considered. The probability distribution for $y_2(0)$ is however different. In particular, ξ is discontinuous on $[a, b] = [-1, 1]$ with a density defined by:

$$f(\xi) = \frac{1}{M} \times \begin{cases} \dfrac{1 + \cos(\pi\xi)}{2} & \text{if } \xi \in [-1, 0] \\ 10 + \dfrac{1 + \cos(\pi\xi)}{2} & \text{if } \xi \in [0, 1] \\ 0 & \text{else} \end{cases} \tag{26a}$$

and $M = 11/2$ to ensure normalization.

Because of the discontinuous pdf, only MC-SOBOL and SI solutions can be compared, showing the great flexibility given by SI method with respect to the form of the pdf. In figure B.2, variance of $y_1(t)$ is reported for the converged solutions obtained with MC-SOBOL and SI. The SI method permits to reproduce exactly MC-SOBOL solution. In figure B.3, a consistency study for SI is reported by using an increasing number of points in the stochastic space. In Table B.3, we reported number of samples required to reach a prescribed error in the L^2 and L^∞ norms. The SI method shows to be very competitive in terms of efficiency and computational cost with respect to MC-SOBOL method when whatever form of pdf is used (a discontinuous pdf in this case), at least for this problem. Let us remark that a uniform grid is used in the stochastic plane: no type of mesh adaptation is considered here. This displays the great potentiality of this method if coupled with an adaptive methods.

3.1.2. 2D KO problem

Then, we use SI method to study the K-O problem with two-dimensional random inputs:

$$y_1(0) = 1.0, \qquad y_2(0) = 0.1\xi_1, \qquad y_3(0) = \xi_2,$$

where ξ_1 is discontinuous on $[a, b] = [-1, 1]$ with a density defined by (26) and ξ_2 is a uniform random variable in [-1,1].

In Figure B.4, the SI capability to reproduce exactly MC-SOBOL solution is represented. The SI and MC-SOBOL solutions are nearly coincident also for long time ($t = 50$). The mesh convergence study in the stochastic space for SI is reported in figure B.5 showing that the solution obtained with a mesh of 320×320 is well converged. In Table B.4, the computational cost required to reach a prescribed error of ϵ_{L^2} is reported. In this particular example, reductions from 50% to 66% are obtained using SI with respect to MC-SOBOL solutions. Once again, let us emphasis that these results have been obtained *without* any mesh adaptation, contrarily to [13]. In our case, adaptivity is doable and certainly much better results in term of cost could be obtained in that case. Our emphasis here is to show the potential of the method without any fancy subtilities and improvements.

3.2. Nozzle flow with shock

The steady shocked flow in a convergent-divergent nozzle is taken into account with a fixed (deterministic) geometry:

$$A(x) = \begin{cases} 1 + 6(x - \frac{1}{2})^2 & \text{for} \quad 0 < x \leq \frac{1}{2} \\ 1 + 2(x - \frac{1}{2})^2 & \text{for} \quad \frac{1}{2} < x \leq 1 \end{cases}$$

The outlet pressure (subsonic outlet flow with $p_e = 1.6529$ bar) is chosen in order to have a compression shock in the divergent part of the nozzle, exactly located at $x = 0.75$. For the other boundary conditions, a subsonic inlet flow with a stagnation pressure $p_0 = 2$ bar and a stagnation temperature $T_0 = 300$ K are considered. The mean value of the ratio of specific heats γ is 1.4. Two test-cases are considered. First, an uncertain heat coefficient ratio γ is assumed. The random parameter $\omega = \gamma$ varies within the range $[1.33, 1.47]$, following various choices of pdf (uniform and discontinuous) described below. In the second test-case, two-uncertainties stochastic problem is solved where γ follows a discontinuous pdf and the subsonic outlet flow varies uniformly within the range $1.6529 \pm 2\%$.

The random parameter ω (defining either the heat ratio or the subsonic outlet flow) ranges between ω_{min} and ω_{max}; the interval $[\omega_{min}, \omega_{max}]$ is mapped onto $[a, b]$ by a linear transformation and the pdf on $[a, b]$ is either:

- uniform with $\omega \in [a, b] = [0, 1]$,
- discontinuous on $[a, b] = [0, 1]$ with the density defined in relation (26).

Again, various stochastic methods are used to compute statistics of the supersonic nozzle. In a first step, a uniform pdf on γ is used in order to compare MC-SOBOL, PC and SI. In a second step, γ follows (26) and we compare MC-SOBOL and SI to demonstrate the flexibility, and the accuracy, offered by the SI method.

After a study on the grid convergence, the 1D physical space is divided in 201 points (with the normalized geometric domain that varies from 0 to 1). The base scheme is a standard TVD scheme using MUSCL extrapolation on the characteristic variables with Roe flux and Harten-Yee entropy fix. The scheme is implicit to speed up the convergence to steady state. The code has been modified along the lines of the algorithm 2. A preliminary convergence study with respect to the stochastic estimation has been realized, by using an increasing refinement of the probabilistic space discretization in the case of the SI method, and an increasing polynomial order in the case of PC method. The probabilistic space discretization varies from 5 to 160 points (in practice: 5, 10, 20, 40, 80, 160 points). For the PC expansion, the polynomial order varies from 2 to 100. For that problem, we have observed that convergence for the mean is already reached at order 10. Next, the stochastic solutions are compared computing the mean and the variance of the Mach number and pressure distributions along the nozzle using various choices of pdf for γ. Finally, a comparison in terms of computational cost is performed by computing error ϵ_{L^2} with respect to x. In Figure B.6, the mean solutions of Mach number and the pressure along the 1D nozzle are reported, where the mean stochastic solutions are computed with the SI method using 10 points in the probabilistic space and the PC method using a 10th order polynomial, with γ described by a uniform pdf (γ varying between 1.33 and 1.47). As can be observed in Figure B.6, the mean flow is characterized by an isentropic region of increasing speed or Mach number between $x = 0$ and the mean shock location in the divergent (the flow becoming supersonic at the nozzle throat located in $x = 0.5$), followed by a subsonic flow behind the shock with decreasing speed. The mean solutions computed by the two UQ methods are coincident. Next the standard deviation of the Mach number is computed along the nozzle by using different refinement levels for the probabilistic space in the case of the SI method and different polynomial order in the case of the PC method, always keeping a uniform pdf for γ. In Table B.5, the number of samples required to reach a prescribed error ϵ_{L^2} is reported for each strategy. The SI method needs fewer points in the stochastic space for a given level of error.

Then, a discontinuous pdf is considered for the stochastic γ. It is interesting to show the kind of innovative contribution the SI method can bring with respect to the PC method (in its classical version). To this end, in Figure B.7, the standard deviation of Mach is reported along the nozzle when the discontinuous pdf defined in equation (26) is considered. Note that choosing the relation (26) to describe the random variable γ introduces no change whatsoever in the application of the SI method while the PC method can no longer be used. The standard deviation of the Mach number distribution computed for this discontinuous pdf is plotted in Figure B.7 for several levels of discretization refinement in the probabilistic space: here again the result can be considered as almost converged with no more than a 40-point discretization and fully converged with a 80-point discretization. In Figure B.8, the standard deviation of the Mach is reported along the nozzle for the discontinuous pdf by using SI and MC-SOBOL methods. The standard deviation distributions computed by means of the SI and MC-SOBOL methods are coincident, even for the maximal standard deviation. The stochastic estimation remains globally very similar for the newly proposed SI approach and the well-established MC-SOBOL method, which allows to validate the SI method results for the case of a discontinuous pdf on γ. Let us estimate the respective computational cost of SI, MC-SOBOL for this case. In Table B.6, the number of samples required to reach a prescribed error in the L^2 and L^∞ norms is reported for the SI and MC-SOBOL methods. A drastic reduction of the computational cost is obtained by using the SI method with respect to MC-SOBOL solutions, again for that particular problem.

Next, a two-uncertainties stochastic problem is considered by assuming a discontinuous pdf for γ and a uniform pdf for p_e. In Figure B.9, the standard deviation of the Mach is reported along the nozzle for SI and MC-SOBOL. The standard deviation distributions computed by means of SI and MC-SOBOL are identical. As shown in Table B.7, the SI method allows strongly reducing the computational cost until six times with respect to MC-SOBOL method.

3.3. Viscous Burgers equation

In this section, we show how higher order reconstruction techniques affect the accuracy of the numerical solution with respect to a reference analytical solution. The aim is to check the inequality (24). Let us consider the viscous Burger's equation

$$\frac{1}{2}\frac{\partial u^2}{\partial x} = \nu \frac{\partial^2 u}{\partial x^2}, \tag{27}$$

where $x \in [0,1]$ and $u(0) = 1$ and $u(1) = -1$. We take

$$\nu = 0.1 + 0.2\big(\cos(2\pi\omega) + 1.\big) \tag{28}$$

with a uniform $\omega \in [0,1]$.

The computation is initialized by using $u^0 = 1 - 2x$ and run up to convergence. For this equation, it is possible to compute exactly the solution $u_\nu(x) = \tanh\left(\frac{x}{2\nu}\right)$ and the associated variance.

Several probabilistic reconstructions have been used, here are our notations for the Figures B.10 and B.11:

- O3 and centered five points: for the cell j, use the cells $j-2$, $j-1$, $j+1$ and $j+2$ (probabilistic indices).
- O2 and centered 3 points : for the cell j, use the cells $j-1$ and $j+1$ (probabilistic indices).
- ENO : ENO reconstruction using the cells j $j-1$ and $j+1$ for the cell j,
- O1 : use the cell j only.

The figure B.10 displays the solution (with a zoom on the right) for $\Delta x = \frac{1}{41}$, $\delta\omega = \frac{1}{11}$.

As expected higher is the formal accuracy, better are the results. In particular, the centered 3 points reconstruction gives the best results with respect to the exact solution while the less accurate solution have been obtained by using the first order reconstruction.

These behavior is confirmed by a convergence analysis, as shown in figure B.11, where the L^2 and L^∞ norms of the variance have been reported for several spatial resolutions. Remark that the error saturates (i.e. if $\delta\omega$ is too large, the main error is the spatial error), and this error decreases when Δx decreases. Finally, these results show how the statistics accuracy can be improved by using an higher reconstruction order in the stochastic space.

3.4. Inviscid airfoil simulation.

We report this example not because the results have a real physical meaning (the simulations are done with an Euler solver) but to show the versatility of the method: the CFD solver is a second order Residual distribution scheme using hybrid unstructured meshes, see e.g. [3, 4]. The geometry is that of a RAE 2822 airfoil. The mesh is quite coarse (3800 vertices). The inflow average Mach number is $M_\infty = 0.8$. The norm of velocity at infinity U_{inf} is random with a fluctuation of $\pm 2\%$ around its average value. The pdf are uniform or Gaussian. The Figure B.12 displays the pressure coefficient.

4. Summary

This paper deals with the formulation of a semi-intrusive (SI) method allowing the computation of statistics of linear and non linear PDEs solutions. This method is said semi-intrusive because it requires only a limited amount of modifications in a deterministic flow solver to quantify uncertainty on the flow state when the flow solver includes uncertain variables. Then, it can be considered as very easy to implement in comparison with other intrusive methods, like as Polynomial Chaos. This method shows to be very efficient to deal with probability density function of whatsoever form, long-term integration and discontinuities in stochastic space. Several test cases have been considered. First, a modified version of the Kraichnan Orszag three-modes problem has been taken into account by considering a discontinuous pdf for the stochastic variable. This test is very challenging seeing that other intrusive methods well known in literature can suffer of long time integration problems even for uniform pdf. The SI method displays good results and a drastic improvement in computational time with respect to Monte Carlo solutions. Secondly, a stochastic nozzle flow has been considered with discontinuous pdf again, where SI shows large reduction of computational cost with respect to Monte Carlo solution. Then, SI has been applied to solve the viscous Burgers equation

with several probabilistic reconstruction of stochastic space. As expected, higher order reconstruction allow to reduce the error by using the same number of points in the stochastic space, displaying the interest to use more accurate reconstruction in order to improve numerical accuracy of statistic properties. The last example, aimed at showing the versatility of the method, is a compressible flow simulation over an airfoil.

Let us emphasis that the results presented in this work have been obtained by using always a uniform grid in the stochastic space without any kind of adaptivity according to the probability density function, showing an interesting potentiality for further improvements.

Adaptivity of the stochastic grid and the coupling with sparse-grid based methods for multi-dimensional problems will be implemented in a future work.

Acknowledgment

Remi Abgrall has been financed in part by the EU ERC Advanced Grant ADDECCO N. 226316. The authors thanks Stéphane Galéra for his contribution in the early stages of this work. We also thanks the unknown referees for their very constructive comments.

References

[1] R. Abgrall. An essentially non-oscillatory reconstruction procedure on finite-element type meshes: Application to compressible flows. *Comput. Methods Appl. Mech. Eng.*, 116:95–101, 1994.

[2] R. Abgrall. On essentially non-oscillatory schemes on unstructured meshes: Analysis and implementation. *J. Comput. Phys.*, 114(1):45–58, 1994.

[3] R. Abgrall. Essentially non-oscillatory residual distribution schemes for hyperbolic problems. *J. Comput. Phys.*, 214(2):773–808, 2006.

[4] R. Abgrall, A. Larat, and M. Ricchiuto. Construction of very high order residual distribution schemes for steady inviscid flow problems on hybrid unstructured meshes. *J. Comput. Phys.*, 230(11):4103–4136, 2011.

[5] R. Abgrall and Th. Sonar. On the use of Mühlbach expansions in the recovery step of ENO methods. *Numer. Math.*, 76(1):1–25, 1997.

[6] N. Agarwal and N. R. Aluru. A domain adaptive stochastic collocation approach for analysis of MEMS under uncertainties. *J. Comput. Phys.*, 228:7662–7688, 2009.

[7] I. Babuska, R. Tempone, and G.E. Zouraris. Galerkin finite elements approximation of stochastic finite elements. *SIAM J. Numer. Anal.*, 42:800–825, 2004.

[8] T. J. Barth and P. O. Frederickson. Higher order solution of the Euler equations on unstructured grids using quadratic reconstruction. In *AIAA paper 90-0013*, pages 1–12. AIAA, 1990.

[9] P. G. Ciarlet and P. A. Raviart. General Lagrange and Hermite interpolation in $\mathbb{R}^n$ with applications to finite element methods. *Arch. Ration. Mech. Anal.*, 46:177–199, 1972.

[10] P.G. Constantine, D.F. Gleich, and G. Iaccarino. Spectral methods for parameterized matrix equations. *SIAM J. Matrix Anal. A.*, 31:2681–2699, 2010.

[11] J. Foo, X. Wan, and G.E. Karniadakis. The multi-element probabilistic collocation method (ME-PCM): error analysis and applications. *J. Comput. Phys.*, 227(22):9572–9595, 2008.

[12] O. Friedrich. Weighted essentially non-oscillatory schemes for the interpolation of mean values on unstructured grids. *J. Comput. Phys.*, 144(1):194–212, 1998.

[13] M. Gerritsma, J. van der Steen, P. Vos, and G.E. Karniadakis. Time-dependent generalized polynomial chaos. *J. Comput. Phys.*, 229(22):8333–8363, 2010.

[14] T. Gerstner and M. Griebel. Numerical integration using sparse grids. *Numer. Algorithms*, 18:209–223, 1998.

[15] R. G. Ghanem and S. D. Spanos. *Stochastic Finite Elements : a Spectral Approach*. Springer Verlag, 1991.

[16] J.M. Hammersley and D.C. Handscomb. *Monte Carlo Methods*. Fletcher & Son Ltd, 1964.

[17] A. Harten, B. Engquist, S. Osher, and S. Chakravarthy. Uniformly high order accurate essentially non-oscillatory schemes. III. *J. Comput. Phys.*, 71:231303, 1987.

[18] T.Y. Hou, W. Luo, B. Rozovskii, and H.-M. Zhou. Wiener chaos expansions and numerical solutions of randomly forced equations of fluid mechanics. *J. Comput. Phys.*, 216:687–706, 2006.

[19] Changqing Hu and Chi-Wang Shu. Weighted essentially non-oscillatory schemes on triangular meshes. *J. Comput. Phys.*, 150(1):97–127, 1999.

[20] R. H. Kraichnan. Direct-interaction approximation for a system of several interacting simple shear waves. *Physics of Fluids*, 6(11):1603–1609, 1963.

[21] X. Ma and N. Zabaras. An adaptative hierarchical sparse grid collocation algorithm for the solution of stochastic differential equations. *J. Comput. Phys.*, 228:3084–3113, 2009.

[22] O.P. Le Maitre, O.M. Knio, H.N. Najm, and R.G. Ghanem. A stochastic projection method for fluid flow, i: Basic formulation. *J. Comput. Phys.*, 173:481–511, 2001.

[23] O.P. Le Maitre, M.T. Reagan, H.N. Najm, R.G. Ghanem, and O.M. Knio. A stochastic projection method for fluid flow. ii. Random process. *J. Comput. Phys.*, 181:9–44, 2002.

[24] H.N. Najm. Uncertainty quantification and polynomial chaos techniques in computational fluid dynamics. *Annu. Rev. Fluid Mech.*, 41:35–52, 2009.

[25] S. A. Orszag and L. R. Bissonnette. Dynamical properties of truncated Wiener-Hermite expansions. *Physics of Fluids*, 10(12):2603–2613, 1967.

[26] G. Poette, B. Despres, and D. Lucor. Uncertainty quantification for systems of conservation laws. *J. Comput. Phys.*, 228:2443–2467, 2009.

[27] M.T. Reagan, H.N. Najm, R.G. Ghanem, and O.M. Knio. Uncertainty quantification in reacting-flow simulations through non-intrusive spectral projection. *Combust. Flame*, 132:545–555, 2003.

[28] P. L. Roe. Approximate Riemann solvers, parameter vectors, and difference schemes. *J. Comput. Phys.*, 43:357–372, 1981.

[29] S. Smolyak. Quadrature and interpolation formulas for tensor product of certain classes of functions. *Soviet Math. Dokl.*, 4:240–243, 1963.

[30] X. Wan and G. E. Karniadakis. An adaptative multi-element generalized polynomial chaos method for stochastic differential equations. *J. Comput. Phys.*, 209(2):617–642, 2005.

[31] X. Wan and G. E. Karniadakis. Long-term behavior of polynomial chaos in stochastic flow simulations. *Computer Methods in Applied Mechanics and Engineering*, 195(1-3):5582–5596, 2006.

[32] X. Wan and G. E. Karniadakis. Multi-element generalized polynomial chaos for arbitrary probability measure. *SIAM J. Sci. Comput.*, 28(3):901–928, 2006.

[33] D. Xiu. Fast numerical methods for stochastic computations: a review. *Communications in Computational Physics*, 5(2):242–272, 2009.

[34] D. Xiu and G. E. Karniadakis. The Wiener-Askey polynomial chaos for stochastic differential equations. *Journal of Science Computing*, 26, 2002.

Appendix A. Error estimate on the recovery step

In this section, we systematicaly identify the subsets $\Omega_j \subset \Omega$ to subsets of $\mathbb{R}^s$ that are still denoted by Ω_j. We pick one (arbitrary) point ω_i in the convex hull of $\cup_{\Omega_l \in \mathcal{S}_i} \Omega_l$ that we denote by convex $(\mathcal{S}_i)$. We first notice that the reconstruction problem (9) keep the polynomials of degree less than p invariant, i.e. given Y a polynomial of degree p, the unique $P \in \mathbb{R}[x_1, \cdots, x_n]$ such that

$$E(X \mid \Omega_j) = \frac{\int_{\mathbb{R}^n} 1_{\Omega_j}(x_1, \cdots, x_n)\, P(x_1, \cdots, x_n)\, d\tilde{\mu}}{\mu(\Omega_i)} \qquad \text{for } j \in \mathcal{S}_i$$

holds true is $P = X$. Then following [9], if X is of class C^r with $r \geq p+1$, we have, in Ω_i

$$X - P = \int_0^1 (1-t)^p D^{p+1} X(\omega_i + t(\omega - \omega_i)) \cdot (\omega - \omega_i)^{p+1} dt.$$

Here, $D^{p+1}X$ is the $p+1$-th derivative of X with repect to the random parameters.

Then, using the regularity of f, we take the expectancies and get

$$\left|E(f(X)|\Omega_i) - E(f(P)|\Omega_i)\right| \leq \max ||D^{p+1}X||_\infty E(||(\omega - \omega_i)^{p+1}||\ |\Omega_i).$$

In this inequality and from the results in [9], the point ω_i, as well as ω belongs to the convex hull of $\cup_{\Omega_l \in \mathcal{S}_i} \Omega_l$. Hence,

$$\left|E(f(X)) - E(f(P))\right| \leq \max ||D^{p+1}X||_\infty \max_{\Omega_i} \min_{\omega_i \in \text{convex}(\mathcal{S}_i)} E(||(\omega - \omega_i)^{p+1}|||\Omega_i). \tag{A.1}$$

We have thus the following result:

Proposition Appendix A.0.1. *If X is of class C^r with $r \geq p+1$ and if f is a real valued function of class C^1, then* (A.1) *holds true.*

Remark Appendix A.1. *A rough estimation of* $\max_{\Omega_i} \min_{\omega_i \in convex(\mathcal{S}_i)} E(||(\omega - \omega_i)^{p+1}|||\Omega_i)$ *is*

$$\max_{\Omega_i} \min_{\omega_i \in convex(\mathcal{S}_i)} E(||(\omega - \omega_i)^{p+1}|||\Omega_i) \leq \left(diameter\ (convex\ (\mathcal{S}_i)\right)^{p+1}.$$

However, this estimate assumes implicitely that each event occur with more or less the same probability. In the case of tails of probability, think of a Gaussian for example, this estimate overestimate the weight of rare events. Hence (Appendix A.0.1) *contains more information than a rough estimate that is reminiscent of standard interpolation.*

Appendix B. Some error estimates about the SI algorithm

We consider the example of an elliptic problem ($\mathcal{O} \subset \mathbb{R}^n$

$$\begin{array}{ll} -\nabla \cdot \big(K(x,\omega)\nabla u\big) = f(x,\omega) & x \in \mathcal{O}, \omega \in \Omega \\ u = 0 & \text{on } \partial\mathcal{O}. \end{array} \tag{B.1}$$

Again, Ω is the set of random variables. It is equipped with a family of measurable sets and a measure μ. In (B.1), we assume that the problem is uniformly coercive: there exist $\alpha_0 > 0$ independent of $(x, \omega) \in \mathcal{O} \times \Omega$ such that for any $x \in \mathbb{R}^n$,

$$x^T \Big(K(x,\omega)x \Big) \geq \alpha_0 ||x||^2.$$

We also assume that there exist a constant M independent of (x, ω) such that

$$\int_{\mathcal{O}} f(x,\omega)^2 dx \leq M.$$

Under these assumptions, for any event ω, the solution of (B.1) belongs to $H_0^1(\mathcal{O})$, satisfies the variational principle: for any $v \in H_0^1(\mathcal{O})$,

$$\int_{\mathcal{O}} \nabla v^T \Big(K(x,\omega) \nabla u(x,\omega) \Big) dx = \int_{\mathcal{O}} f(x,\omega) v(x) dx,$$

and there exist a (uniformly) bounded operator $\mathcal{A}(\omega)$ such that

$$u(\ .\ ,\omega) = \mathcal{A}(\omega) f(\ .\ ,\omega)$$

To make things easier, $\mathcal{O}$ is assumed to have a polygonal boundary. The domain $\mathcal{O}$ is discretized by a conformal triangulation $\mathcal{T}_h$, and the approximation space V_h is

$$V_h = H_0^1(\mathcal{O}) \cap \{ v \text{ continuous}, v_{|T} \in \mathbb{P}^1(T) \}$$

Then using the previous assumptions, there exist a constant C, independent of Ω such that the numerical solution u_h satisfies

$$||u_h - u||^2_{H_0^1(\mathcal{O})} := \int_{\mathcal{O}} \big(\nabla u_h - \nabla u \big)^2 dx \leq C h^2.$$

From this, we have

$$\begin{aligned}
\int_{\mathcal{O}} \Big(\nabla E(u_h|\Omega_i) - \nabla E(u|\Omega_i) \Big)^2 dx &= \int_{\mathcal{O}} E\big(\nabla (u_h - u|\Omega_i) \big)^2 dx \\
&\leq \int_{\mathcal{O}} E\Big(\big(\nabla (u_h - u) \big)^2 |\Omega_i \Big) dx \text{ by Cauchy- Schwartz inequality and } E(1|\Omega_i) = 1 \\
&= \int \Big(\int_{\mathcal{O}} \Big(\nabla (u_h - u) \Big)^2 dx \Big) d\mu(|\Omega_i) \text{ by Fubini} \\
&\leq C h^2
\end{aligned} \tag{B.2}$$

One can show similar error estimates on the L^2 norm.

Unfortunately, one does not solve (B.1) in one shot, but with an iterative method. Setting U^n the vector of components u_j^n, the iterative method (for the deterministic solver) writes

$$U^{n+1} = JU^n + b$$

where the iteration matrix J will depend on the finite element space and the matrix K. We assume here that $||J||_{L^p} < 1$ uniformly in ω for some p. Let us give the example of the Jacobi method. From the variational formulation of (B.1), we have for any vertex

$$\sum_{j \in \mathcal{O}} c_{ij} (u_i - u_j) = F_j \tag{B.3}$$

with

$$c_{ij} = \int_{\mathcal{O}} \nabla\varphi_i^T \Big(K \nabla\varphi_j \Big) dx, \qquad F_j = \int_{\mathcal{O}} f\varphi_i \, dx$$

where the φ_j are the standard piecewise linear shape functions. The Dirichlet boundary conditions are automaticaly satisfied if the index j corresponds to interior nodes only. It is well known that for any i only a finite number of c_{ij} are non zero, they correspond to the vertices j connected to i by an edge. Under geometrical conditions, one can show that $c_{ij} \geq 0$. In the case of the Jacobi method, we have

$$J_{ij} = \left\{ \begin{array}{ll} 0 & \text{if } j = i \\ \frac{c_{ij}}{\sum_k c_{ik}} & \text{else.} \end{array} \right.$$

We have $||J||_\infty \leq 1 - \alpha$ where α is independent of ω under standard assumptions on the mesh. The right hand side b is given by $b_i = F_i / \sum_k c_{ik}$. To study the effect of this algorithm on the method, we see that with exact integration, we would have

$$\text{for all } i, E(u_i^{n+1}|\Omega_k) = \sum_j E(c_{ij} u_j^{n+1}|\Omega_k) + E(b_i|\Omega_k).$$

This algorithm converges to $E(u_i|\Omega_k)$ where $u_i(\omega)$ is the limit of the Jacobi algorithm for ω frozen because the error $e_{ik}^n = E(u_i^n|\Omega_k) - E(u_i|\Omega_k)$ satisfies

$$e_i^{n+1} = \sum_j E(J_{ij} e_j^n|\Omega_k)$$

and then

$$||E(e^{n+1}|\Omega_k)||_{L^1} = \sum_j |E((Je^n)_i|\Omega_k)| \leq (1-\alpha)||e^n||$$

since $|E(e_j^n|\Omega_k)| \leq E(|e_j^n| \, |\Omega_k)$.

In the case of approximate integration, the terms $E(c_{ij} u_j^n|\Omega_k)$ are evaluated by quadrature formula from a reconstruction of u^n as explained in the main section of the paper. Since the number of j for which $c_{ij} \neq 0$ is bounded above uniformly if the mesh is regular, we see that the error is bounded by $\epsilon_\ell := C(u) \times \max_{\Omega_i} \min_{x_i \in \text{convex}(\mathcal{S}_i)} E(||(x - x_i)^{\ell+1}|||\Omega_i)$ where ℓ is the degree of the polynomial reconstruction, $\Delta\omega$ is the mesh size in the random direction and C is a constant that depends on the regularity of $\omega \mapsto u_j(\omega)$, see appendix Appendix A. This means that

$$E(u_i^{n+1}|\Omega_k) = \sum_j E(c_{ij} u_j^n|\Omega_k) + b_j + \epsilon_\ell.$$

From this we get estimates

$$E(||e^{n+1}||_{L^1}|\Omega_k) \leq (1-\alpha) E(||e^n||_{L^1}|\Omega_k) + C\epsilon_\ell,$$

and then by induction

$$E(||e^{n+1}||_{L^1}|\Omega_k) \leq (1-\alpha)^n E(||e^0||_{L^1}|\Omega_k) + C\Big(\sum_{j=1}^n (1-\alpha)^j \Big) \epsilon_\ell.$$

This shows that numerical integration only add an $C(u) \times \max_{\Omega_i} \min_{x_i \in \text{convex}(\mathcal{S}_i)} E(||(x - x_i)^{\ell+1}|||\Omega_i)$ error and explain the observation of section 3.3, though it is not the same PDE.

Figures

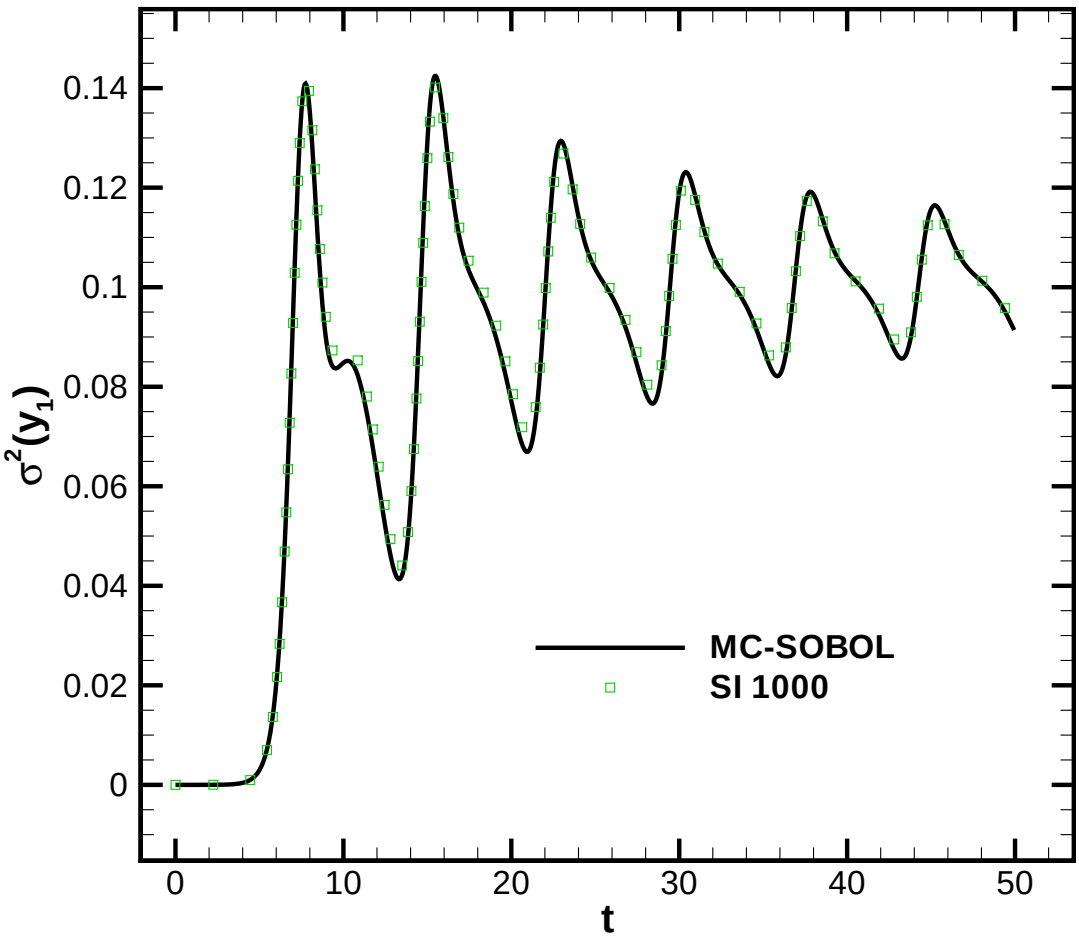

Figure B.2: Variance of y_1 computed by means of SI and MC-SOBOL methods.

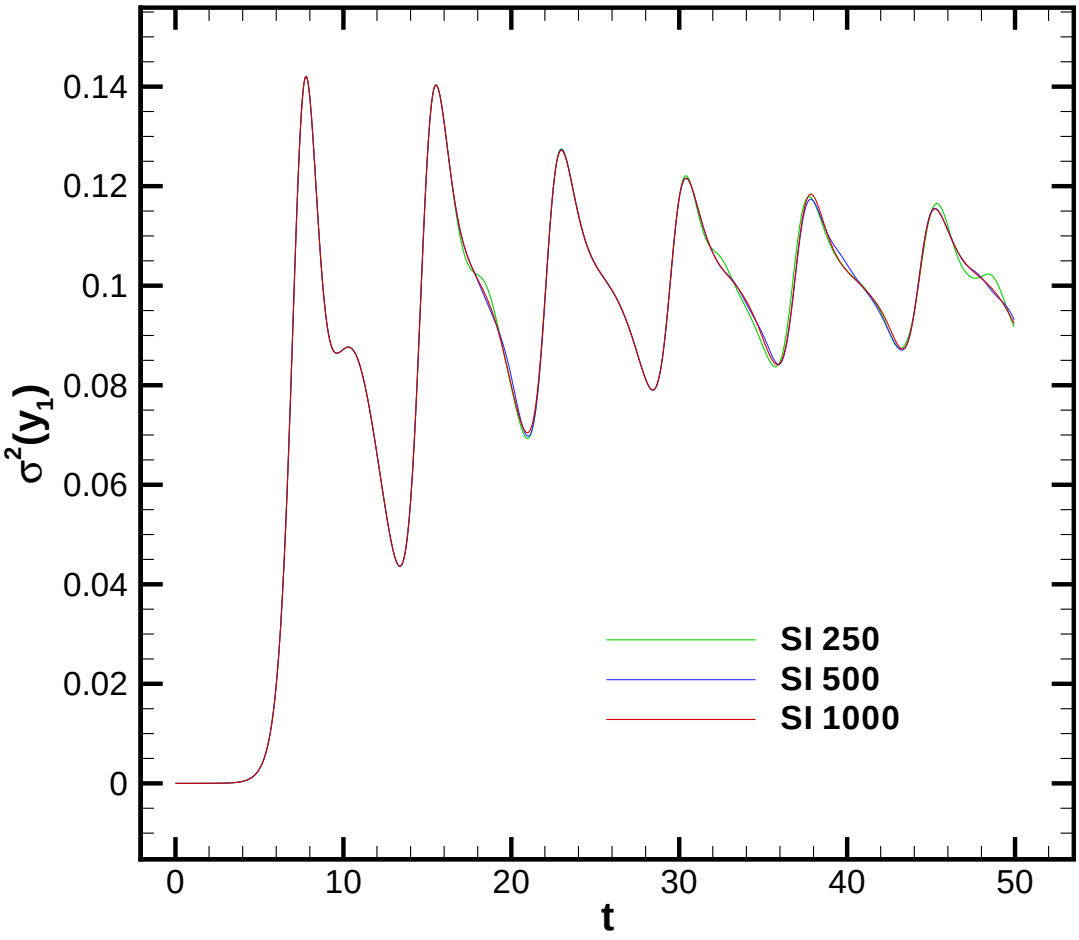

Figure B.3: Variance of y_1 computed by means of SI for different meshes in the stochastic space.

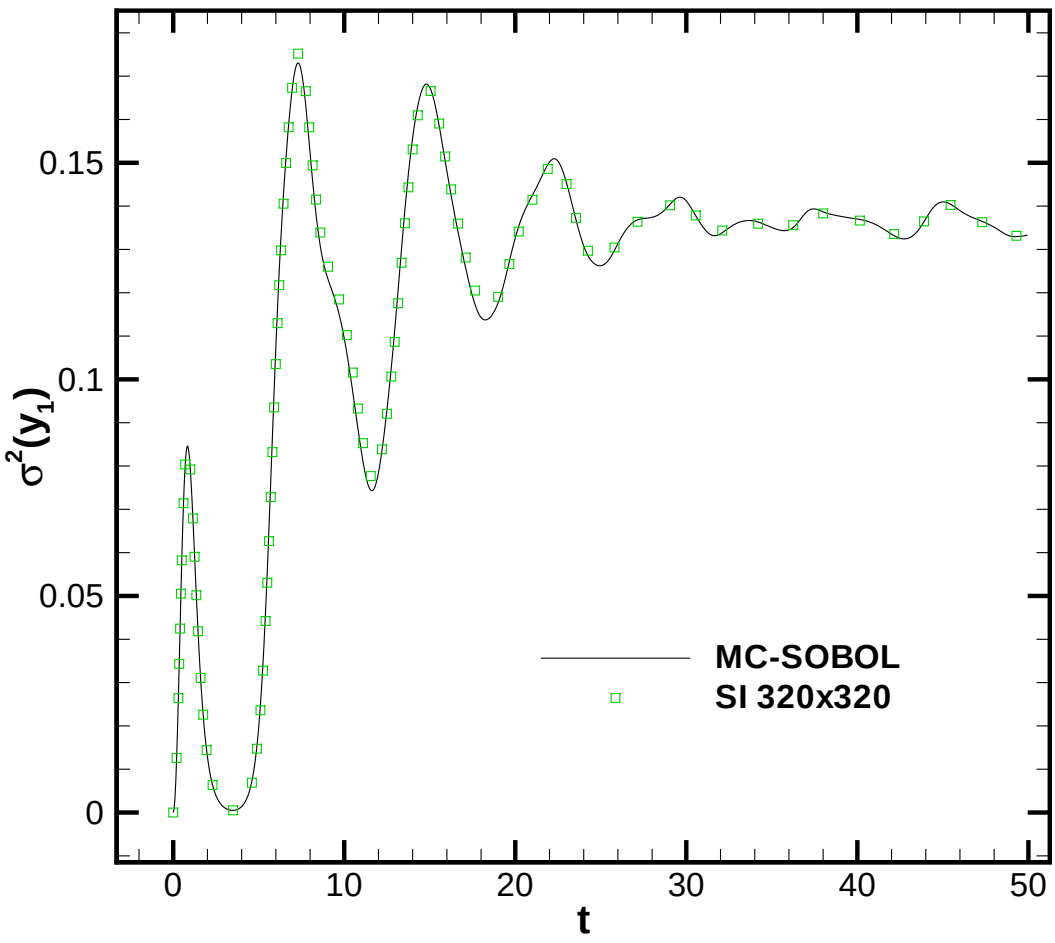

Figure B.4: Variance of y_1 computed by means of SI and MC-SOBOL methods.

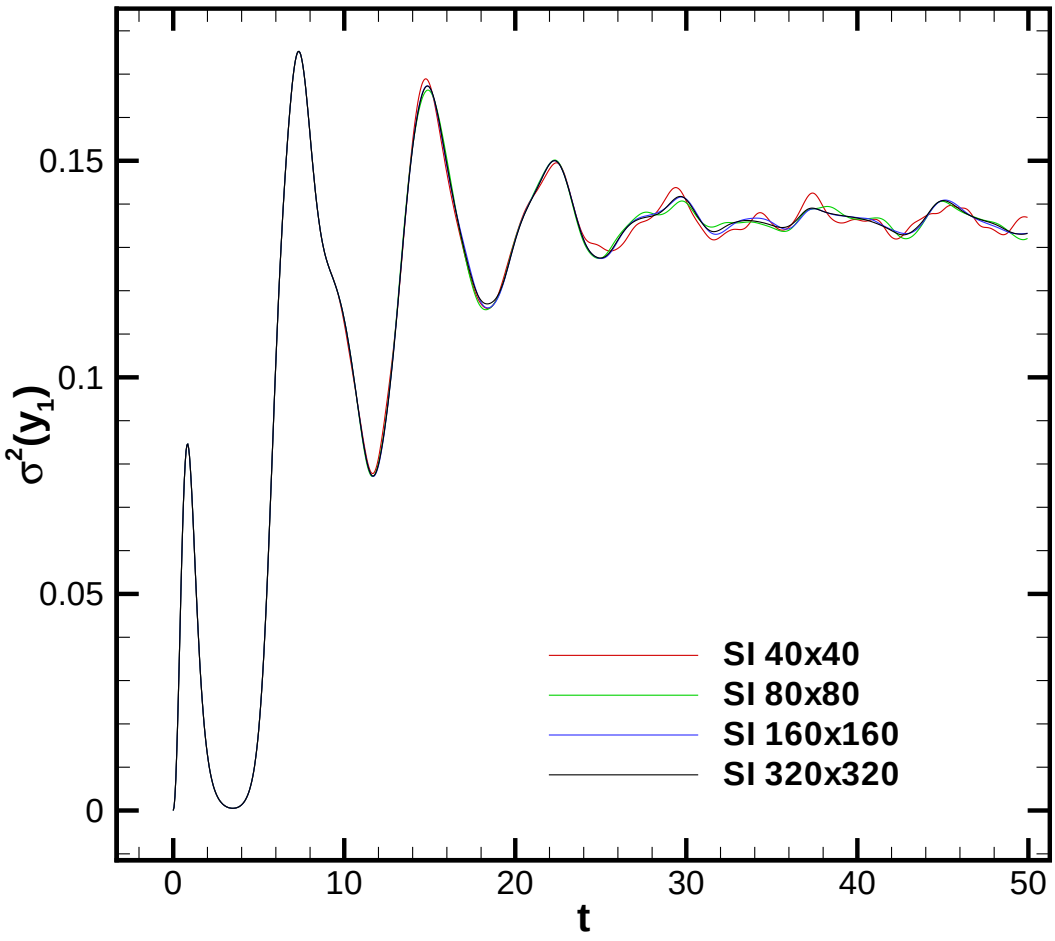

Figure B.5: Variance of y_1 computed by means of SI for different meshes in the stochastic space.

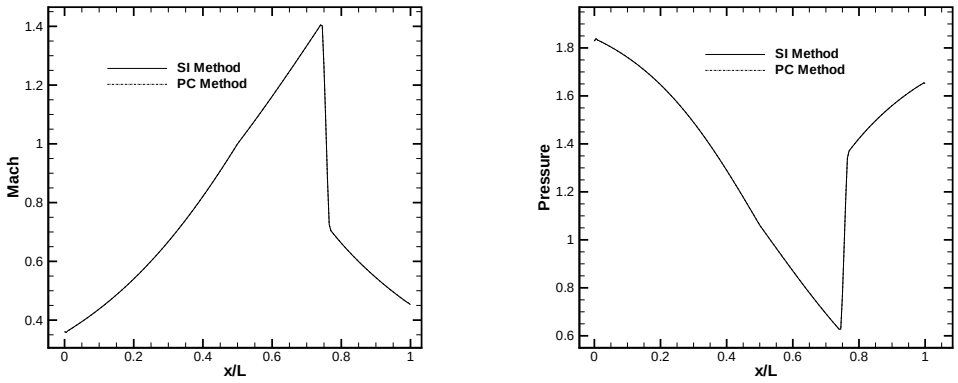

Figure B.6: Nozzle flow with uncertain γ (uniform pdf). Computed mean distribution for the Mach number (left) and the static pressure (right) using the semi-intrusive method with 10 points in the probabilistic space and the PC method with a 10th order polynomial.

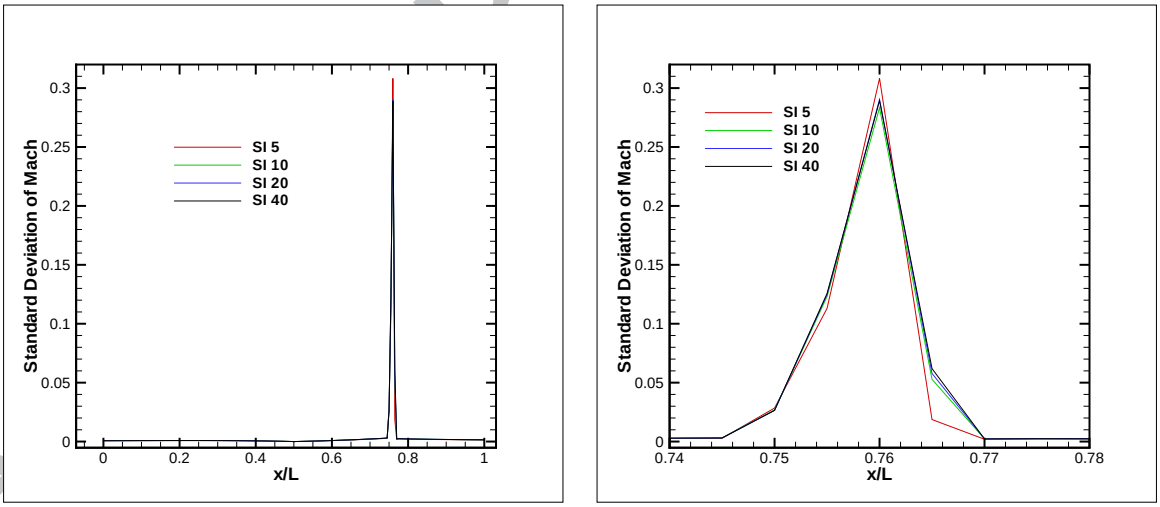

Figure B.7: Nozzle flow with uncertain γ (discontinuous pdf). Convergence study for the standard deviation on the Mach number distribution computed using the SI method.

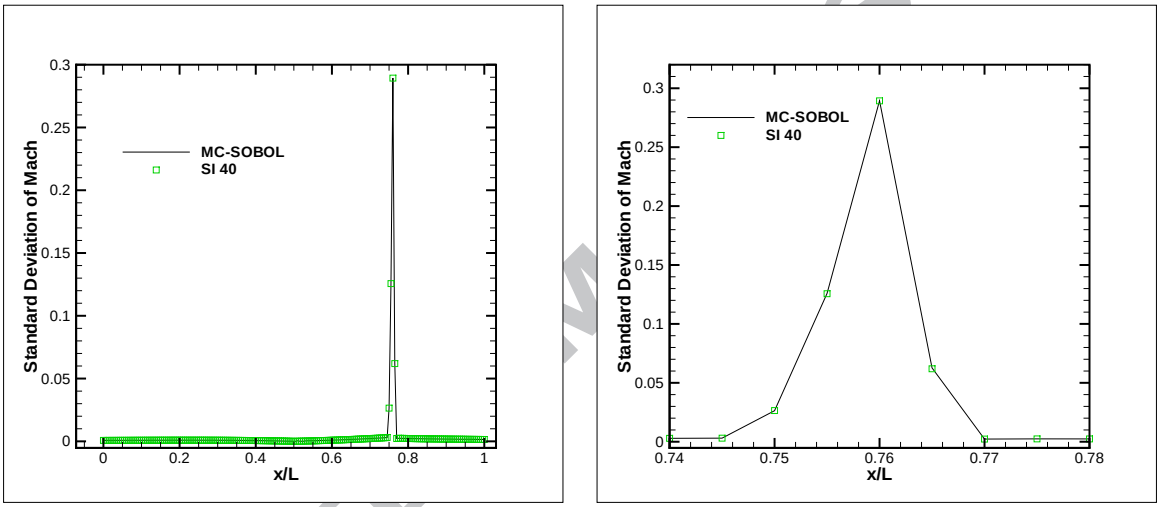

Figure B.8: Nozzle flow with uncertain γ (discontinuous pdf). Standard deviation for the Mach number distribution for MC-SOBOL and SI methods. Left : global view; right : close-up on the shock region.

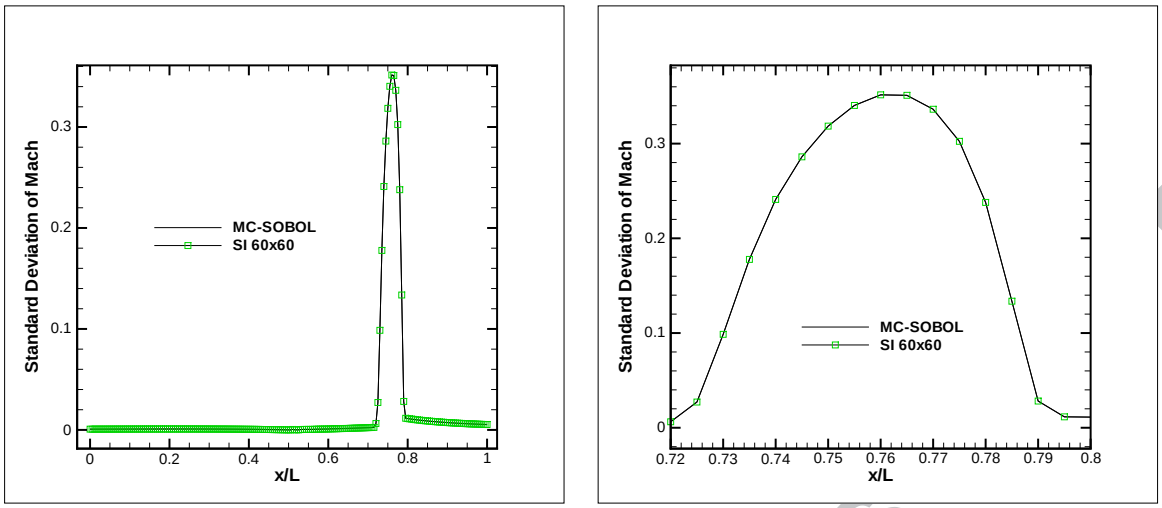

Figure B.9: Nozzle flow with uncertain γ (discontinuous pdf) and p_e (uniform pdf). Standard deviation for the Mach number distribution for MC-SOBOL and SI methods. Left : global view; right : close-up on the shock region.

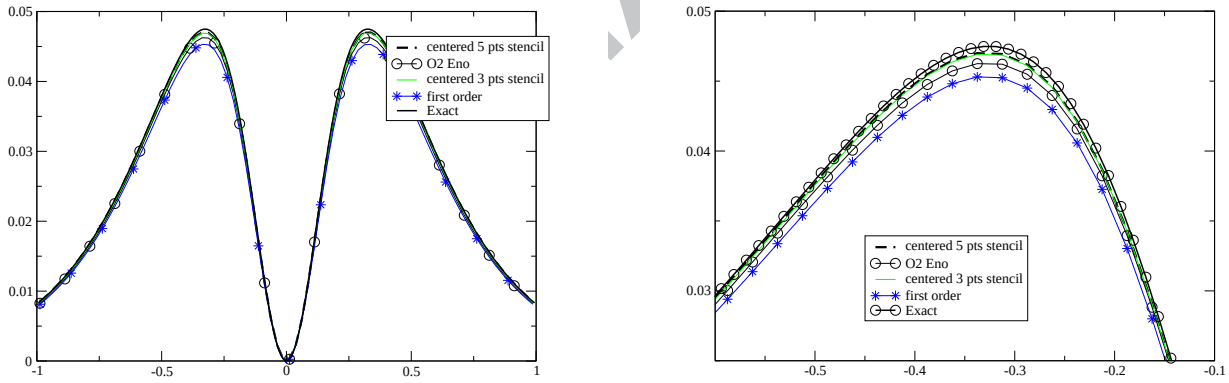

Figure B.10: For a fixed spatial resolution and a fixed "probabilistic" resolution, comparison of the O3,O2,ENO and first order reconstructions. The exact variance is obtained from the exact solution with $\Delta x = 1/160$ and $\Delta\omega = 1/40$.

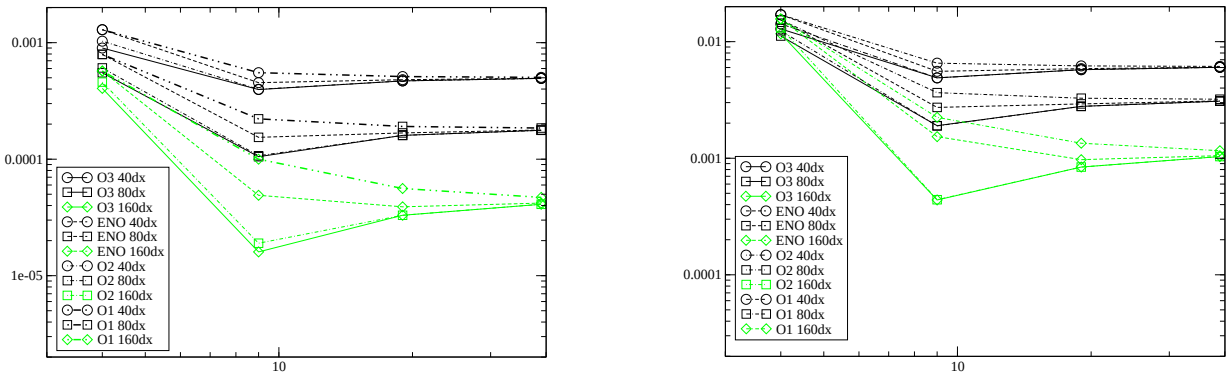

Figure B.11: For the O3,O2,ENO and first order reconstruction, evaluation of the (spatial) L^2 and L^∞ norms of the variance for the spatial resolutions of $\Delta x = 1/40, 1/80, 1/160$. Left : L^2 norm, right :L^∞ norm

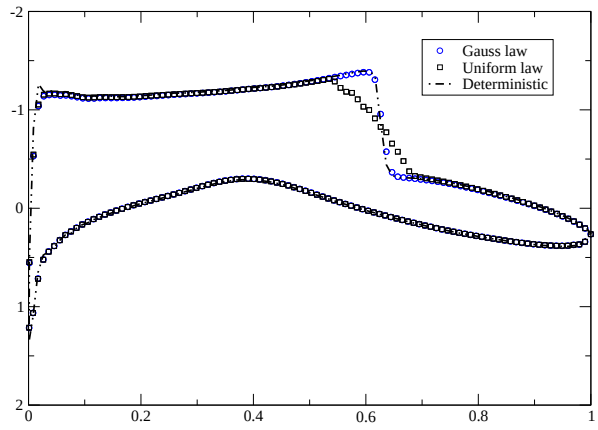

Figure B.12: Pressure coefficient of the deterministic solution with $M_\infty = 0.8$, and when a Gaussian or a uniform law is applied on the inflow velocity.

Tables

Error level ϵ_{L^2}	MC-SOBOL	PC	SI	Error level ϵ_{L^∞}	MC-SOBOL	PC	SI
10^{-1}	20	12	5	10^{-1}	75	24	24
10^{-2}	240	19	10	10^{-2}	520	37	36
10^{-3}	2200	23	20	10^{-3}	4500	85	82

Table B.2: Number of samples required for the 1D K-O problem for time $t \in [0, 10]$. The errors are given in the L^2 (left) and L^∞ (right) norms.

Error level ϵ_{L^2}	MC-SOBOL	SI	Error level ϵ_{L^∞}	MC-SOBOL	SI
10^{-1}	35	7	10^{-1}	60	15
10^{-2}	250	160	10^{-2}	450	240
10^{-3}	2500	900	10^{-3}	3500	1400

Table B.3: Number of samples required for the 1D-discontinuous K-O problem for time $t \in [0, 50]$. The errors are given in the L^2 (left) and L^∞ (right) norms.

Error level ϵ_{L^2}	MC-SOBOL	SI	Error level ϵ_{L^∞}	MC-SOBOL	SI
10^{-1}	160	81	10^{-1}	400	170
10^{-2}	10000	2500	10^{-2}	18000	4000
10^{-3}	300000	102400	10^{-3}	400000	160000

Table B.4: Number of samples required for the 2D-discontinuous K-O problem for time $t \in [0, 50]$. The errors are given in the L^2 (left) and L^∞ (right) norms.

Error level ϵ_{L^2}	MC-SOBOL	PC	SI
10^{-1}	5	6	5
10^{-2}	24	19	10
10^{-3}	70	59	40

Table B.5: Number of samples required for the 1-uncertainty nozzle problem, uniform pdf.

Error level ϵ_{L^2}	$MC-SOBOL$	SI
10^{-1}	4	5
10^{-2}	42	20
10^{-3}	250	40

Table B.6: Number of samples required for the 1-uncertainty nozzle problem, discontinuous pdf.

Error level ϵ_{L^2}	MC-SOBOL	SI
10^{-1}	35	25
10^{-2}	1000	400
10^{-3}	20000	3600

Table B.7: Number of samples required for the 2-uncertainties nozzle problem, discontinuous pdf .

Algorithms

Algorithm 1 Flow chart for the deterministic scheme (7).

Initialize U^0
for n:= 1 to $nmax$: Deterministic loop **do**
From U^n, evaluate the relevant parameters V^n for the solver $\Im$,
Evaluate $\Im(V^n) = U^{n+1}$.
end for

Algorithm 2 Flow chart for the system (15). The deterministic sequence are underlined, they corresponds to the steps of the deterministic algorithm 1.

for j:=1 to $jmax$: Probabilistic loops **do**
Evaluate U_j^0, the initial condition.
end for
for $n := 1$ to $nmax$: Deterministic loop **do**
for j:=1 to $jmax$: Probabilistic loops **do**
For each Ω_i, evaluate the reconstruction polynomial $R(U^n)_i(x, \omega)$.
for $j^{quad} := 1$ to j_{max}^{quad} : Quadrature loop: **do**
Evaluate the relevant parameters $V^n_{j^{quad}} = R(U^n)_i(x, \omega_{j^{quad}})$
Evaluate $\Im(V^n_{j^{quad}}) = U^{n+1}_{j^{quad}}$.
end for
From the $\{U^{n+1}_{j^{quad}}\}_{j^{quad}}$, evaluate U^{n+1} from the quadrature formula (11).
end for
end for

Algorithm 3 Flow chart for the system (15). The deterministic steps are underlined

for n:= 1 to $nmax$: Deterministic loop **do**
  for j:=1 to $jmax$: Probabilistic loops: **do**
    for $j^{quad} := 1$ to j^{quad}_{max} : Quadrature loop: **do**
      Reconstruct a piecewise polynomial $u^n_{j_{quad}}(x)$ of $u^n(x, X(\omega))$ in each cell Ω_j
      for $i := 1$ to i_{max} : Deterministic loop **do**
        reconstruct a piecewise polynomial $u^n_{i,j^{quad}}$ of $u^n_{j^{quad}}(x)$ in each cell C_i
        Compute fluxes $F(u^n_{i+1,j_{quad}}, u^n_{i,j_{quad}})$, ... using deterministic solver
        Control time step $\Delta t_{\Omega_{j_{quad}}}$
      end for
    end for
    compute expectancies $E(F(u^n_{i+1}, u^n_i)|\Omega_j)$, ... using quadrature formula
    update probabilistic time step $\Delta t_{\Omega_j} = \min_{\Omega_{j_{quad}}}(\Delta t_{\Omega_{j_{quad}}})$
  end for
  update total time step $\Delta t = \min_{\Omega_j}(\Delta t_{\Omega_j})$
  for $j := 1$ to j_{max} : Probabilistic loop **do**
    for $i := 1$ to i_{max} : Deterministic loop **do**
      update values

$$u^{n+1}_{i,j} = u^n_{i,j} + \frac{\Delta t}{|C_i|}\Big(E(F(u^n_{i+1}, u^n_i)|\Omega_j) - E(F(u^n_i, u^n_{i-1})|\Omega_j)\Big)$$

    end for
  end for
end for